Available online at www.sciencedirect.com
SCIENCE DIRECT®
Journal of Magnetic Resonance 169 (2004) 174–186
JMR Journal of Magnetic Resonance
www.elsevier.com/locate/jmr

Thin film MRI—high resolution depth imaging with a local surface coil and spin echo SPI

Alexei V. Ouriadov, Rodney P. MacGregor, and Bruce J. Balcom*

Department of Physics, MRI Centre, University of New Brunswick, P.O. Box 4400, Fredericton, NB, Canada E3B 5A3

Received 2 September 2003; revised 14 April 2004

Abstract

A multiple echo, single point imaging technique, employing a local surface coil probe, is presented for examination of thin film samples. Depth images with a nominal resolution of 5 μm were acquired with acquisition times on the order of 10 min. The method may be used to observe dynamic phenomenon such as polymerization, wetting, and drying in thin film samples. It is readily adapted to spatially resolved diffusion coefficient and T_2 relaxation time mapping.

Keywords: Pure phase encode; Spin echo; SPI; Depth imaging; Thin film; Nafion; Drying; Polymerization; Diffusion coefficient; T_2; Relaxation time mapping; Wetting

1. Introduction

The last few decades have seen the development of a wide range of very powerful and flexible surface analysis techniques and instrumentation [1]. There is no doubt that the chemical and physical properties of many materials are determined by the surface. However, it is also true that frequently the region of interest in a material may be more rationally thought of as an interfacial layer with finite thickness, say hundreds of microns. Problems of this type quite naturally occur in the wetting, drying or polymerization of surface coatings. Thin film problems of this type, with analysis as a function of depth from the surface, are not amenable to study by the vast majority of current surface science instrumentation.

In the case of wetting, drying or polymerization one is naturally interested in the behavior of liquid or liquid-like phases associated with a solid substrate and spatially resolved magnetic resonance MRI, is a natural approach to the problem.

The current gold standard for thin film MRI is the Stray Field technique (STRAFI) developed by Peter MacDonald and co-workers [2–5]. The STRAFI method is based on the use of a strong, constant, magnetic field gradient from the periphery of permanent or superconducting magnets. The fixed gradient in STRAFI while necessary for high resolution imaging of short T_2 samples does entail several significant disadvantages.

The intense gradient means that the MRI signal will always have a large bandwidth, even for liquid-like species with reasonable T_2 values. For liquid-like samples, the intense gradient ensures that signal intensity will always be reduced due to molecular self-diffusion. In addition the intense frequency encoding gradient ensures off-resonance RF pulse excitation with the result that echo trains in STRAFI do not behave in a simple exponential manner. Finally, the magnet origin of the STRAFI gradient requires that a planar sample be physically leveled to ensure the gradient is orthogonal to the film surface.

In this paper, we introduce a thin film imaging technique which will be highly complimentary to STRAFI. It is not suitable for short T_2 thin film imaging but will be advantageous for imaging thin film liquid-like systems. As will be demonstrated, it has inherently good SNR due to a relatively narrow signal bandwidth and therefore optimal digital filtering. Lacking magnetic

* Corresponding author. Fax: +1-506-453-4581.
E-mail address: bjb@unb.ca (B.J. Balcom).

1090-7807/$ - see front matter © 2004 Elsevier Inc. All rights reserved.
doi:10.1016/j.jmr.2004.04.015

field gradients at the k-space origin, the experimental image will not suffer from diffusive attenuation [6]. The echo decay is simply governed by T_2, simplifying the image contrast. By exploiting 3D magnetic field gradients in a standard imaging instrument, it is possible to 'level' the sample by controlling the effective magnetic field gradient orthogonal to the thin film surface—without physical movement of the sample. In addition 3D magnetic field gradients permit a ready experimental check on the sensitive region of the experiment.

2. Theory

2.1. Surface coil

High resolution thin film imaging requires radio frequency probes which are inherently capable of high signal to noise ratio (SNR) imaging. According to Eq. (1), the SNR [7–9] is improved by maximizing the B_1 field per ampere of excitation current, B_1/I, while minimizing the effective excitation volume, V_{eff} of the probe [9]

$$\text{SNR} \propto \frac{B_1/I}{\sqrt{\Delta f \text{Res} V_{\text{eff}}}}. \tag{1}$$

The coil resistance and the probe bandwidth are variables Res and Δf, respectively, in Eq. (1).

A small surface coil is the natural approach to maximizing B_1/I while minimizing V_{eff} [9,10]. As illustrated in Fig. 1, a local surface coil positioned immediately above or below the film of interest naturally defines a cylindrical sample volume. One may envision averaging over the cylindrical area to resolve depth with better SNR.

Naively one would imagine that the volume excited by the surface coil will reflect the probe diameter and the sample thickness. One must, however, consider the B_1 field distribution within the thin film in order to understand the behaviour of the proposed measurement

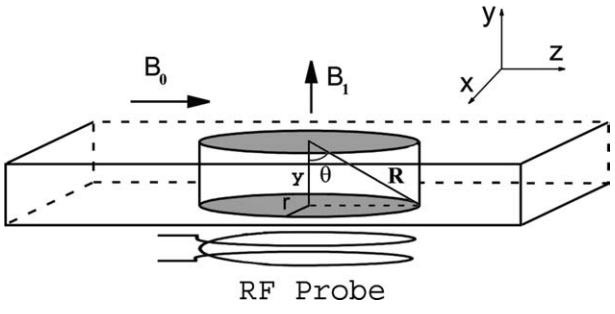

Fig. 1. Penetration of a thin film sample by the B_1 field in the case of a surface coil probe. The surface coil radii is r, y is the axial distance, and R is the distance to the observation point from the origin. The true coordinate origin is the surface coil center, not the sample bottom as represented in the figure.

$$B_1 = \frac{\mu_0 I r^2}{2R^3} \cdot (a_r 2\cos\theta + a_\theta \sin\theta). \tag{2}$$

Eq. (2) describes the magnetic field created by the loop of wire in spherical coordinates. The field depends on the probe current I, surface coil radius r, permeability of free space μ_0, R is the distance from our coordinate origin to a point of interest in the film, and θ is the angle between R and the vertical y [11].

Fig. 1 shows the R origin at the film surface, for ease of illustration. In reality the R origin will be set by the centre of the RF probe. In general the film thickness will be small compared to the probe diameter, and the film center will be displaced from the probe a distance chosen to be $r/2$.

The B_1 variation within the thin film automatically ensures the sample will experience a range of excitation flip angles, as well as variable sensitivity for signal reception.

2.2. Double phase encoding multiple spin echo single point imaging

The choice of pulse sequence was driven by the necessity of obtaining high-resolution depth images of thin film samples—which feature very low inherent signal intensity. The absence of a pulsed magnetic field gradient during data acquisition makes spin echo single point imaging (SPI) [12,13] a natural choice. The lack of gradient permits a very narrow filter and due to this significantly improved image SNR.

Consider 1D spin echo SPI and frequency encode spin echo (SE) methods in terms of SNR. The optimal bandwidth for frequency-encoding is $n(\pi T_2^*)^{-1}$, where n is the number of pixels, while the optimal bandwidth for spin echo SPI is $(\pi T_2^*)^{-1}$ [6,8]. The k-space data point SNR is inversely related to the filter width FW, which should be set to the signal bandwidth in either case, according to Eq. (3)

$$\text{SNR} \propto 1/\sqrt{FW}. \tag{3}$$

From Eq. (3) it is possible to show that $(\text{SNR})_{p.e.} \cdot (SNR)^{-1}_{f.e.} = \sqrt{n}$. This means that the SNR for frequency-encoding is decreased a factor of $\sqrt{n}$ compared to pure phase encoding. After $N = n$ frequency encode signal averages the SNR will be equal for both techniques [6]. If less than N signal averages for frequency-encoding are required then it is the more sensitive technique. In the case of an inherently low SNR system, such as the thin film problem, N signal averages for frequency-encoding may yield inadequate SNR, in which case pure phase-encoding is more sensitive.

If one seeks a nominal pixel resolution better than 5 μm, it is necessary to apply quite a strong magnetic field gradient and consequently one can expect significant signal loss due to molecular self-diffusion with a

conventional frequency encoding spin echo [6,8]. The attenuation $A(k)$ in Eq. (4) is exponential

$$A(k) = \exp\left(-\frac{2}{3}k^2 Dt\right), \tag{4}$$

with D the self-diffusion coefficient, $k = (2\pi)^{-1}\gamma G(\mathrm{TE}/2)$, and $t = \mathrm{TE}$.

The pure phase encoding spin echo will have no diffusive attenuation of the magnetic resonance signal due to imaging gradients, because the mean image amplitude is determined by the magnitude of the signal at the center of k-space ($k = 0$), where the imaging gradient is set to zero [6]. The influence of self-diffusion on the image resolution for spin echo SPI will be considered later in the text.

The family of proposed spin echo SPI [13] pulse sequences are illustrated in Fig. 2. The simplest implementation of spin echo SPI is shown in Fig. 2A. The use of two phase-encoding gradients of opposite polarity [14] permits a decreased encoding time (t_p) and consequently reduces the echo time (TE) by a factor of 2 (Fig. 2B) for identical resolution compared to the single gradient case. This yields an increased [6] magnetic resonance signal when compared to a single phase encoding experiment. Eq. (5) describes the relationship between $S(k)$ and ρ_0 for a 1D T_2-weighted spin echo SPI measurement

$$S(k_y) = \int \rho_0 \exp[-\mathrm{TE}/T_2] \exp[\mathrm{i}2\pi k_y \cdot y]\,\mathrm{d}y, \tag{5}$$

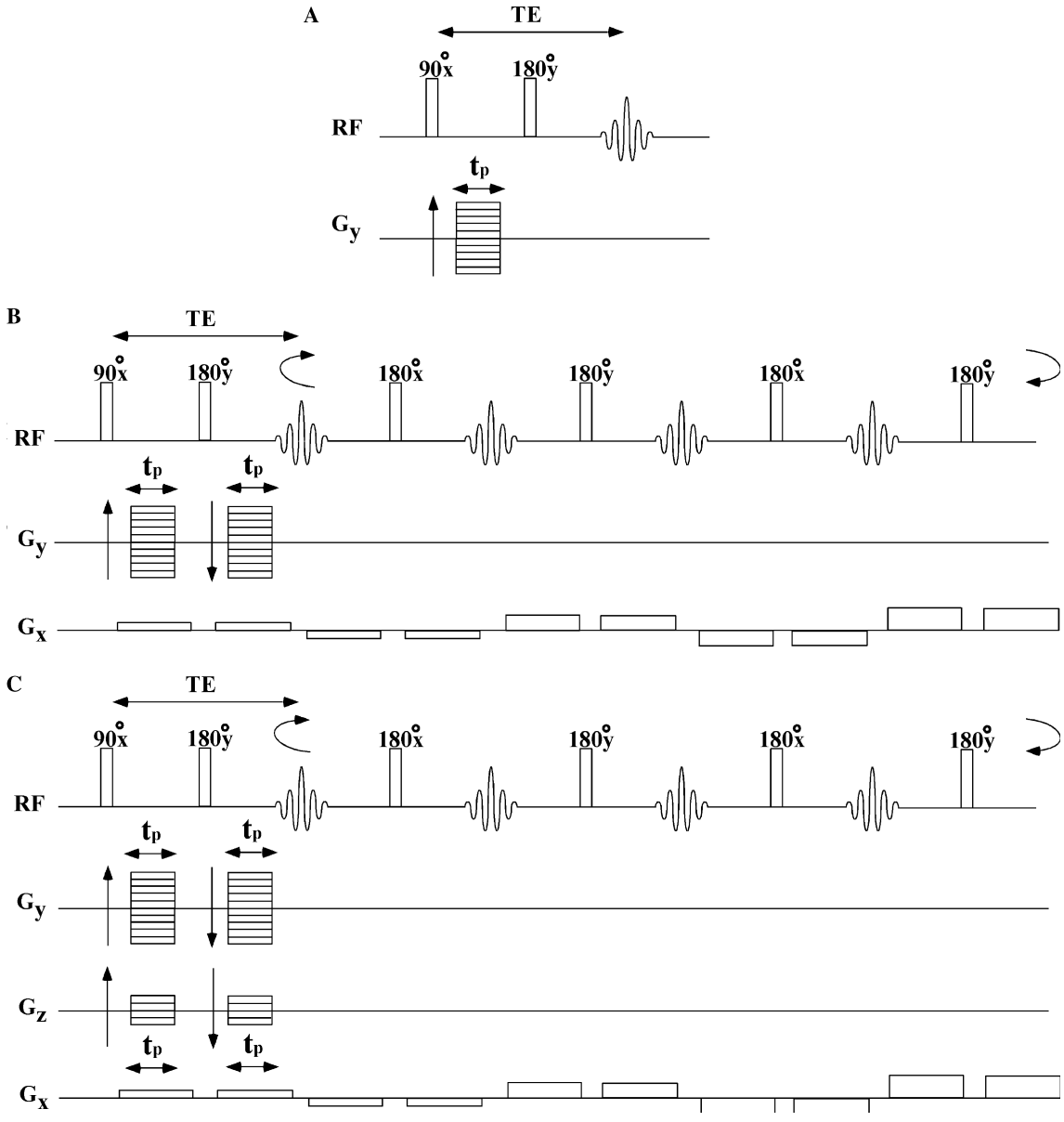

Fig. 2. (A) Pure phase encode, 1D, spin echo SPI sequence. (B) Double phase encode, multiple echo spin echo SPI version of (A) with spoiling gradients. (C) Spin echo SPI pulse sequence as in (B) but with a second phase encode gradient.

where ρ_0 is the nuclear spin density and $k_y = (2\pi)^{-1}\gamma G_y t_p$. The image intensity following Fourier transformation is thus:

$$\rho(y) = \rho_0 \cdot \exp\left(-\frac{\mathrm{TE}}{T_2(y)}\right), \tag{6}$$

where $\rho(y)$ is the apparent nuclear spin density reduced from the true spin density by the T_2 decay.

The addition of multiple echoes (Fig. 2B), to the basic sequence permits the acquisition of multiple T_2 weighted images. The use of a surface coil probe entails inhomogeneous B_1 fields, and thus non-ideal 180° and 90° pulse lengths [10] as discussed earlier. A CPMG sequence in this circumstance [15] will lead to a mixture of magnetization components, an accumulation of phase errors, and the loss of signal. The XY-4 phase cycle [16] proposed in [15] compensates for these pulse length imperfections, without mixing magnetization components.

The inhomogeneous B_1 will also yield an undesirable residual FID in the spin echo train of Fig. 2B. Unwanted spin echoes, forming due to the refocused residual FID, may be avoided by the addition of spoiling gradients (Fig. 2B) calculated according to the Crawley, Wood, and Henkelman formula [17].

3. Results and discussion

3.1. Nominal pulse lengths for SE

The proposed method is based on a spin echo, therefore the determination of nominal 90° and 180° pulse lengths is important. Section 2 shows there will be a significant B_1 variation within the sample. Therefore, one must investigate the manifestation of the flip angle distribution on the measurement.

Fig. 3 shows the pseudo-FID as a function of pulse length for the surface coil probe exciting a thin nafion film. The plot has a pronounced maximum (near 16 μs) and minimum (near 32 μs). This suggests that even though true 90° pulses are impossible to define experimentally for the entire sample, nominal 90° and 180° pulses are reasonably well defined. The true 90° pulse width for a small idealized sample placed in the centre of the surface coil probe was 13 μs for identical pulse power. The simulated pseudo-FID intensity for representative thin layers, accounting for the B_1 field distribution, has qualitatively the same behavior as that revealed in Fig. 3.

3.2. Planar 2D surface coil images

Simulating the 2D sensitivity of the measurement in a plane parallel to the surface coil plane, helps one to predict the influence of inhomogeneous B_1 magnetic fields on the lateral sensitivity of the measurements. It is well known that the magnetic resonance signal for a spin

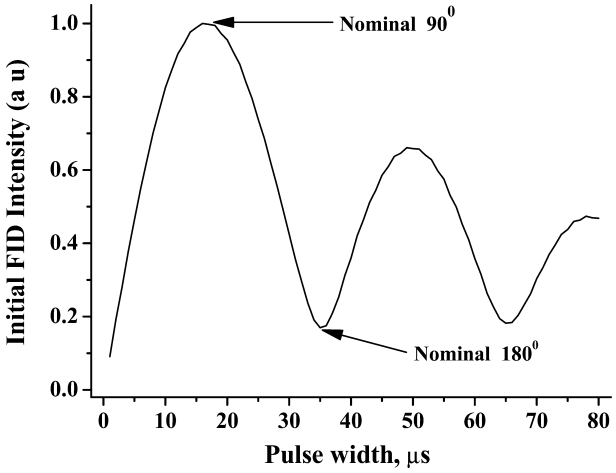

Fig. 3. Pseudo-FID as a function of B_1 pulse width for the surface coil probe with a nafion sample 3×3 cm. The true 90° pulse length for a small sample at the probe centre was 13 μs.

echo measurement, assuming no transverse relaxation, can be calculated [18] from the following equation:

$$S \propto \sin\vartheta_1 \sin^2(\vartheta_2/2), \tag{7}$$

where ϑ_1 is the first flip angle and ϑ_2 is the second flip angle in a spin echo experiment. Spin echo simulations based on the Biot-Savart law, Eq. (7) ($\vartheta_2 = 2\vartheta_1$), and the principle of reciprocity, were undertaken at multiple initial Fig. 3 pulse lengths. The B_1 components orthogonal to B_0 were numerically calculated using the Biot-Savart law for $y = r/2$. Minimal B_1 variation with height y within representative thin films was observed. We henceforth simply assume $y = r/2$ in all calculations and examine instead the significant variation of B_1 laterally within the film. The sample was subdivided into a 4097×4097 element matrix. Spin echo amplitudes were calculated for each pixel. The simulation results are reported as an 'image,' Figs. 4A and B, with the field of view set to twice the surface coil diameter.

The Fig. 4A image, ϑ_1 set to the nominal 90° pulse lengths, has a largely uniform intensity inside the surface coil with an image size that is slightly larger than the surface coil diameter. When angle ϑ_1 was set to the nominal 180° pulse length Fig. 4B, minimal signal intensity was observed within the centre of the surface coil. Fig. 4B clearly shows the calculated image has an ellipsoidal shape.

The ellipsoidal sensitive spot revealed in the simulations of Figs. 4A and B and experiments of Figs. 4C and D is a simple consequence of the experimental geometry illustrated in Fig. 1. The y component of the B_1 flux, at right angles to B_0, is the principal source of sample excitation. However, diverging flux of the B_1 field ensures there will also exist both x and z components. The z components are parallel to the B_0 excitation. The x component will, however, lead to sample excitation and henceforth signal detection. Fig. 4 reveals an elongation of the sensitive spot

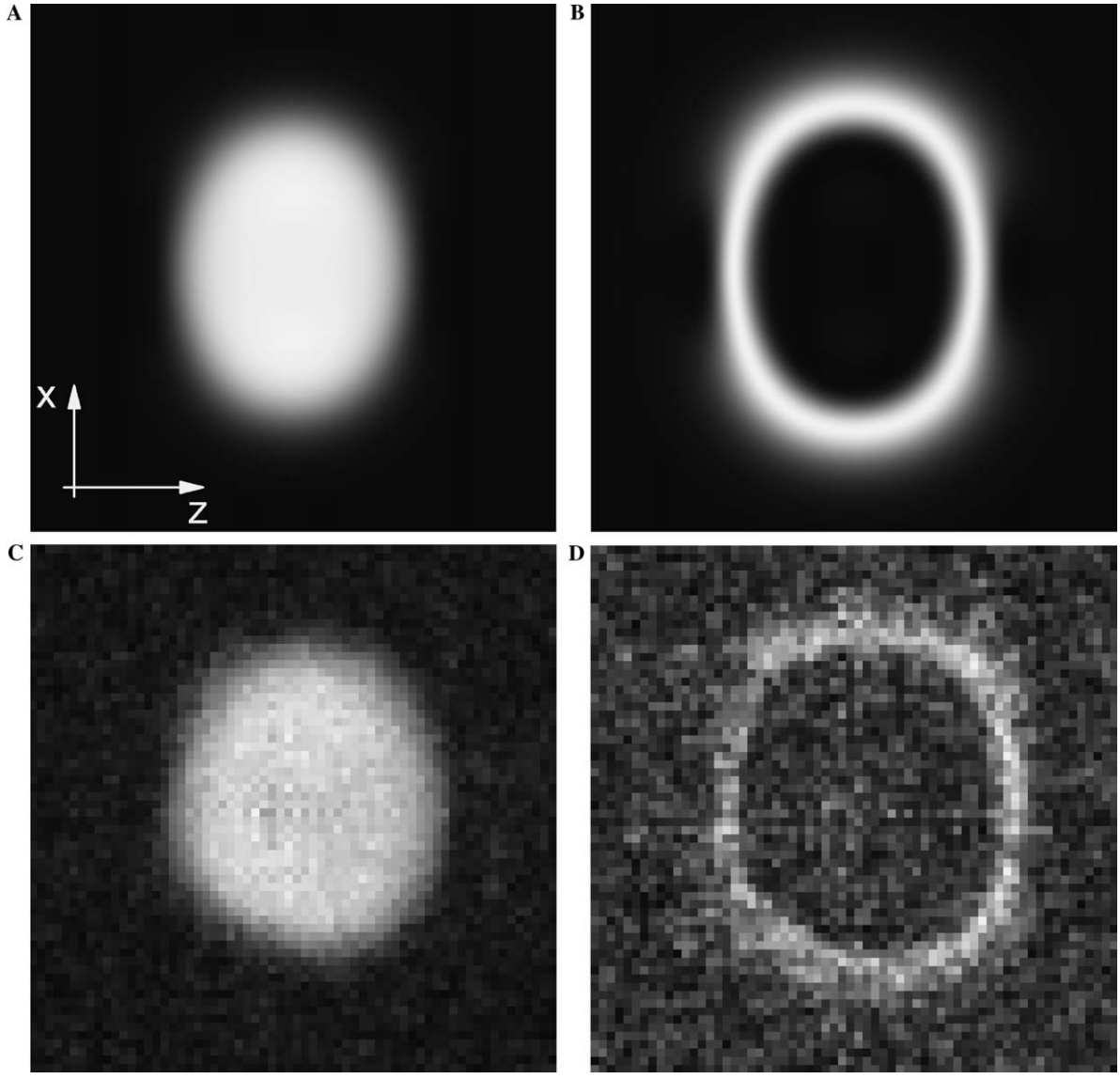

Fig. 4. (A) Calculated 2D signal intensity distribution in the sample plane, parallel to the surface coil probe. The 2D image was calculated from the Biot-Savart law, Eq. (7) and the principle of reciprocity. The first pulse, 14 μs, was set close to the nominal 90° pulse, Fig. 3, for the whole sample. The simulated image intensity is uniform within the surface coil area. The axes illustrated refer to geometry of Fig. 1. (B) 2D signal intensity distribution calculated as per (A) but with the first pulse, 28 μs, set close to the nominal 180° pulse length. A signal intensity void is observed inside the surface coil area. (C) Lateral 2D image of a hydrated nafion sheet parallel to the surface coil probe. Sample size was $3 \times 3\,\mathrm{cm}^2$. The first pulse width was set close to the nominal 90° pulse length. The image shows a reasonably uniform intensity inside the surface coil area. A high resolution depth measurement will average over the sensitive spot directly imaged in this figure. (D) Lateral 2D image of the same nafion sheet, but with the first pulse width set close to the nominal 180° pulse length. The image shows intensity outside the surface coil area. The image has an ellipsoidal shape as observed in the simulation (B).

in the x direction due to the influence of x component of B_1. These effects were incorporated into all simulations.

The simulations predict that lateral averaging over the sensitive spot will yield optimal SNR, and a reasonably uniform lateral sensitivity, in a spin echo SPI depth measurement with pulse lengths chosen to be nominal 90° (ϑ_1) and 180° (ϑ_2) pulses.

Experimental lateral 2D images of the nafion film are shown in Figs. 4C and D. The hydrated nafion film is a thin film sample with uniform proton density. The image represents a projection of the sample on the lateral XZ plane. Fig. 4C, first pulse length set to the nominal 90°, shows a remarkably uniform signal intensity inside the surface coil. The high intensity region of the image corresponds to the surface coil area. The nafion sample is substantially larger than the surface coil diameter and thus the image of Fig. 4C is a direct measure of the sensitive spot.

The edge definition of the sensitive spot and relatively uniform sensitivity within the spot, can be rationalized

by the competitive effects of the variable B_1 field intensity when the nominal 90° and 180° pulse lengths are set longer than the true 90° and 180° pulse lengths. While the B_1 field will be strongest at the sample centre and thus the measurement more sensitive in this region of space, the flip angles will be non-ideal and the transverse magnetization reduced compared to signal further away from centre. Some distance away from the centre, the transverse magnetization will be a maximum due to ideal pulse lengths but the observed signal reduced because of a decreased local B_1 field. In the case of the first pulse set to the nominal 180° pulse length, Fig. 4D, minimal signal intensity is observed within the centre of the surface coil. The experimental image has an ellipsoidal shape and once more confirms the simulated result.

Simulations and experiment show that, fortuitously, satisfactory sensitive spots exist over a broad range of nominal pulse flip angles. The best defined, and most sensitive, spot corresponds to the use of bulk sample nominal 90° and 180° pulse lengths. These effects are the subject of ongoing investigation. In general we may state that spin echo SPI depth measurements will average over a lateral sensitive spot with reasonably uniform sensitivity, with a size that is approximately that of the surface coil.

3.3. High resolution nafion depth images

The profile of Fig. 5A demonstrates that the spin echo SPI technique, Fig. 2B, is capable of high resolution depth imaging. The hydrated nafion layer was 200 μm thick and, 3 cm by 3 cm laterally (Table 2). The image was acquired in 8 min with a SNR of 57. Nafion, a form of perfluorosulfonic acid, is a hydrophilic ionic polymer with ^{1}H relaxation times of the water phase which are reasonably long, T_1, 100 ms, T_2, 13 ms [19,20] and ideally suited to this measurement.

Note the significant blurring of the edges of the depth image, which correspond to the top and bottom of the sheet. This reveals a significant degradation of the true image resolution, compared to the nominal resolution of 4.2 μm. This could occur because the sample does not have a perfectly flat surface, or more likely because the sample plane and phase-encoding gradient are not at right angles. We consider the latter problem in more detail.

Assume the planar sample has a flat surface but the angle between sample and phase-encoding gradient direction is not 90°. Fig. 5D shows an apparent sample thickness (h_1), which can be described by the following equation:

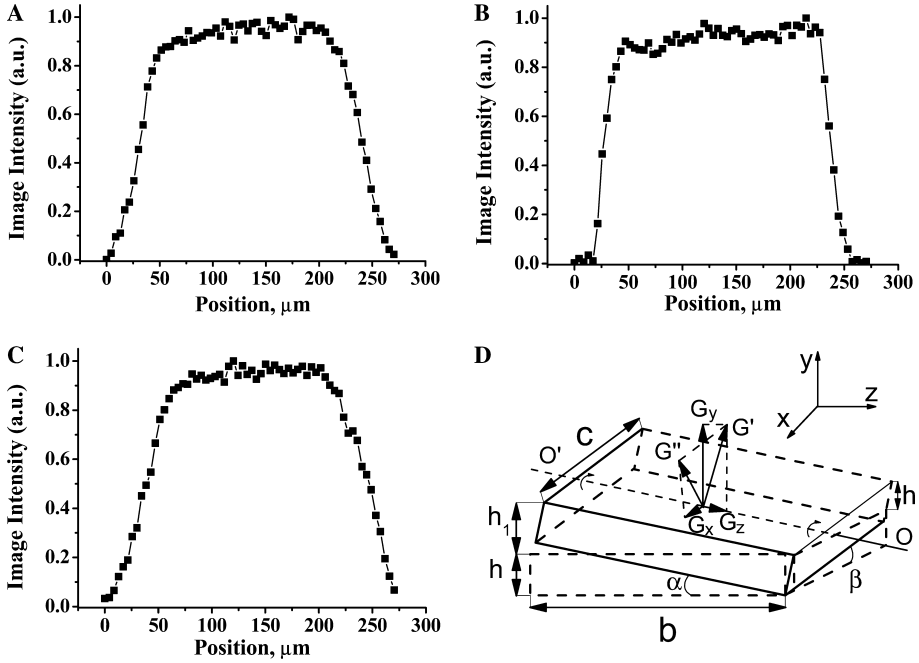

Fig. 5. (A) Depth image of a hydrated nafion film. The angle α was set to 0°. The image was derived from the first echo. Thickness of sample was 200 μm. The non-orthogonality of sample surface and phase encode gradient leads to significant image blurring. (B) As per (A) but with $\alpha = 0.35°$. Note the increased edge resolution achieved by using a near optimal linear combination of the primary and secondary phase encode gradients. (C) As per (A) but with $\alpha = 0.75°$. Note the decreased edge resolution compared to (B). In this case α over compensated for non-orthogonality of the sample and gradient. (D) Non-orthogonal alignment of sample and gradients will lead to blurring of depth profiles. The thin film geometry, sample dimensions and image blurring are linked through angles α and β. The sample thickness is h, b is the length of the sample, while c is the sample width. The variable h_1 is the value of the apparent increase in sample thickness. G', G'' are the resultant phase encoding gradients. The rotation about OO' is angle β.

$$h_1 = \sin\alpha \cdot \sqrt{b^2 + h^2}, \tag{8}$$

where b is the sample length, h is the sample thickness, and α is the angle between the direction of the phase encoding gradient and sample. In the general case there is one more angle β (Fig. 5D), and consequently

$$h_2 = \sin\beta \cdot \sqrt{c^2 + h^2}, \tag{9}$$

where c is the sample width. The values of b and c will be defined by the surface coil diameter (of order of a centimeter) and the typical value of h will be hundreds of micrometers. Thus assuming that the values of α and β are small

$$h_{ap} = h_1 + h_2 = b \cdot \alpha + c \cdot \beta, \tag{10}$$

where h_{ap} is the apparent sample thickness. We will consider in detail only angle α, assuming for other reasons that $\beta = 0$.

Note that in the case of a nafion film, an angle of α of only 1° will cause an increase in the apparent sample thickness of 170 μm. This is comparable to the thickness of the nafion film (Table 1)! A similar sample blurring or sample alignment problem is encountered in Stray field imaging [2–4]. Mechanical leveling is employed in the Stray field technique.

If a small angle α exists between the thin film sample and the horizontal, a very logical solution is to apply an additional small phase encoding gradient as shown in Fig. 2C. If we vary the relative value of the second phase encoding gradient (G_z) it is possible to choose a net gradient $G' = G_y + G_z$ (Fig. 5D) which will be orthogonal to the sample surface. In this case $h_1 = 0$ and consequently the image will have minimal blurring.

The same approach can be used to avoid the β angle problem. As can be seen from Fig. 5D, $G'' = G' + G_x$, so if we change the magnitude of the G_x phase encoding gradient, it is possible to rotate G'' by angle β to eliminate any remaining non-orthogonality. In this work, however, the angle β problem was solved by simple rotation of the planar sample. The probe may be simply and reasonably rotated around the axis OO'. Fixing the RF probe at the gradient face with a marked position ensured reliable probe sample insertion with minimal β angle.

Further nafion depth images are displayed in Figs. 5B and C, employing the pulse sequence of Fig. 2C. The profiles presented have a nominal pixel resolution of 4.2 μm. Images were derived from the first echo. Fig. 5B shows a near optimal linear combination of G_y and G_z, $\alpha = 0.35°$, with significantly increased edge resolution. An additional increase in the relative G_z leads to blurring and an apparent increase in sample thickness (Fig. 5C, $\alpha = 0.75°$). This is quite natural because the resulting gradient G' becomes non-orthogonal to the sample surface with over correction.

Spin echo SPI, when properly executed, permits high resolution 1D depth images of liquid-like thin film samples with a nominal pixel resolution of approximately 4 μm. The best resolution will require a second phase encode magnetic field gradient, the relative value of which must be experimentally determined. How fast might this procedure be undertaken? Speed will be critical if one is attempting to resolve dynamic phenomena in thin films with high spatial resolution. Trial images with variable α permit one to choose an optimal α in less than 10 min.

3.4. Resolution limits

Having demonstrated high resolution depth images, it is important to discuss the resolution limit of the method. It is logical to consider first the question of the influence of the surface coil diameter on the achievable resolution. Increasing the coil diameter by a factor of 2, other factors constant, should improve the experimental signal be a factor of 4 because our 'pixels' are essentially very large flat disks.

Increasing the probe diameter will of course make the measurement more sensitive to non-orthogonality of the gradient and sample. It will be very difficult to completely compensate two independent angles between the gradient and the thin film sample by applying a second and potentially third gradient. If there are uncompensated angles $\Delta\alpha$ and $\Delta\beta$, the residual apparent sample thickness can be estimated from Eq. (10)

$$\Delta h_{ap} = d \cdot (\Delta\alpha + \Delta\beta), \tag{11}$$

where d is the surface coil diameter. Increasing the coil diameter by a factor of 2 immediately increases the

Table 1
Sample parameters

	Length (cm)	Width (cm)	Thickness	T_2^* (ms)	T_2 (ms)	T_1 (ms)
Nafion	3	3	~200 μm	3.5	13	100
Polyurethane coating[a]	2	2	~200 μm	3.5–0.3	12–3	150–90
Polymer latex emulsion[a]	3	0.5	~150 μm	4.1–1.7	29–9	215–180
Balsa wood[b]	3	0.5	0.20 cm	—	—	—
Doped water	3	0.4	~180 μm	6.0	—	50
Micro capillary	3	0.4	~180 μm	—	—	—

[a] Relaxation times for the polyurethane coating and polymer latex emulsion are reported for the beginning and end of the measurement.
[b] The relaxation times of the solid state are typically very short and were not measured.

apparent sample thickness by the same factor. The use of a large diameter surface coil probe will significantly increase the sensitivity, but at the expense of resolution. Conversely, decreasing the surface coil diameter at the expense of sensitivity, will permit an increased resolution according to Eq. (11).

While the current nominal resolution of 4 μm may seem quite modest in comparison to other imaging modalities, and it is limited to 1D, it is of the order of the very best resolution achievable by any MRI technique. Pennington and co-workers [21,22] have achieved 2 μm resolution, at high field with pure water phantoms, and 100 μm or smaller RF coils. Acquisition times of many hours were still required.

It should be technically possible to achieve 2 μm per pixel depth resolution through optimizing the surface coil diameter and better compensation of α and β. At this level one must consider molecular self-diffusion, which is often considered the ultimate resolution restriction in MRI. Cory and co-workers [8] have examined the effect of molecular self-diffusion in a 3D SPI measurement for water samples when the nominal pixel resolution was 5 μm. The full width half maximum (FWHM) of the diffusion point spread function (PSF) was approximately 1 pixel for a self-diffusion coefficient of 2×10^{-9} m^2/s. This FWHM value [8] is less than the theoretical minimum FWHM of 1.21 pixels due to the finite sampling of the data. An analogous calculation may be undertaken for spin echo SPI. For liquid-like polymer samples, the self-diffusion coefficient of which will be less than 10^{-9} m^2/s, the FWHM will be less than 1 pixel for a nominal resolution of 4 μm and approximately 1.5 pixel for a nominal resolution of 2 μm at an echo time of 10 ms.

The realistic resolution limit will, however, often be determined by irregularities in the film surface. The resolution issue must then be examined experimentally on a case by case basis.

3.5. Time resolution of dynamic phenomenon

The previous sections reveal that the spin echo SPI technique permits artifact free, high resolution 1D depth images of planar samples. One logical use of this method is the observation of dynamic phenomenon in thin film samples, for example the processes of polymerization and drying of coatings and adhesives [3,4,23,24].

As an early test of these ideas experiments were undertaken with a polyurethane coating and latex emulsion. The liquid polyurethane coating was applied on a glass substrate. The glass surface was nominally flat. The top surface will naturally be more irregular. 1D depth images of the polyurethane coating obtained over 20 h are reported in Fig. 6. Images were derived from the first echo. The experimental images have only one sharp edge in the image, close to the glass substrate as expected. There is significant blurring on the exposed surface of the polyurethane coating. The profiles show it is possible to observe the loss of water along with the process of time resolved polyurethane coating polymerization leading to a decreased image intensity, and a decreased profile thickness as polymerization proceeds.

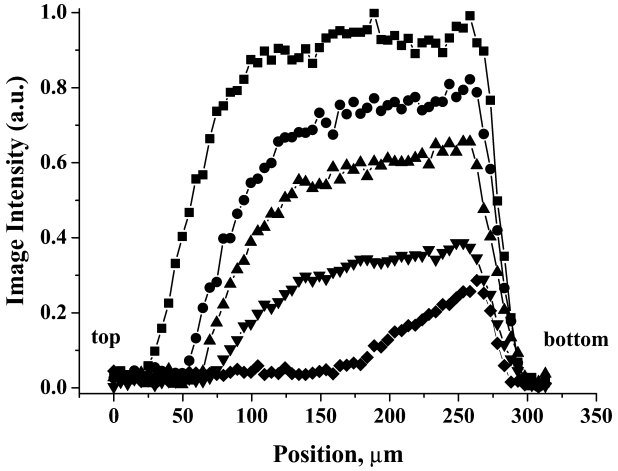

Fig. 6. Observation of polyurethane coating polymerization. 1D depth images were obtained for polyurethane coating on a glass substrate. The sample thickness was approximately 200 μm. Images were derived from the first echo. The first image (■) was obtained immediately after coating the glass substrate. Subsequent images (●, ▲, ▼, and ◆) correspond to 1, 2, 4, and 20 h of curing/drying. The glass interface yields a sharp profile edge (right side). The air-exposed surface has a presumably more irregular surface, therefore it is blurred at time 0. The decreased image intensity and reduced thickness with time shows the combed effects of drying and polymerization.

Polymer latex emulsion, commonly used in carpenter's wood glue, is composed of small vinyl acetate polymer droplets surrounded by water molecules. The process of polymerization requires that polymer droplets coalesce. The process of forming a solid glueline requires that the water molecules leave the emulsion system. This may occur due to drying or, for example, due to adsorption of water by the neighboring material.

A polymer latex emulsion was dispersed between two pieces of balsa wood. This sample does not have regular planar surfaces, due to the nature of the wood. The nominal pixel resolution (10 μm) was decreased by increasing the image FOV. The latex emulsion is observed to be a broad band with diffuse edges. 1D high resolution depth images obtained over 12 h are reported in Fig. 7. The image intensity decreases with time due to adsorption of water by the wood, or transport through the open ends of the wood polymer composite structure.

3.6. Efficiency of data collection

The resolution of dynamic phenomena immediately suggests that the efficiency of data collection will be important. For this reason we compare thin film spin

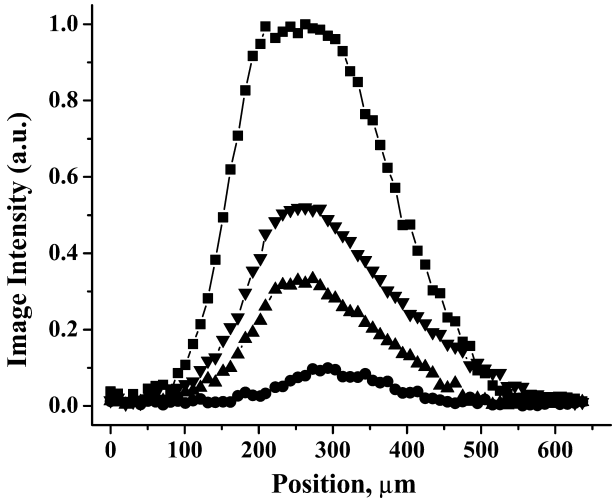

Fig. 7. Observation of polymer latex emulsion polymerization. Depth images were obtained for polymer latex emulsion between two pieces of balsa wood. The sample thickness was approximately 250 μm. Images were derived from the first echo. The first image (■) was obtained immediately after applying the polymer latex emulsion to the balsa wood. Subsequent images (▲, ●, and ▼) correspond to 1.5, 4, and 12 h of curing. The sample does not have a flat surface and therefore the image is significantly blurred. The decreasing image intensity, shows the loss of water along with the process of polymer formation.

echo SPI to analogous frequency encode SE and STRAFI measurements.

A conventional frequency-encoding spin echo experiment for a nafion film with FOV = 500 μm and TE = 14 ms, TR = 300 ms was executed. The same experimental set up was used as for spin echo SPI. No signal was observed even after 256 averages. Conventional frequency-encoding is not effective for obtaining high resolution depth images of thin films. Diffusive attenuation of the frequency encoding spin echo, $A(k)$ can be calculated from Eq. (6) with FOV = 500 μm, TE = 14 ms and a water self-diffusion coefficient of 2×10^{-9} m^2/s. The calculated value of $A(k)$ is 0.2. Frequency-encoding with SE, in this case, ensures that one automatically looses 80% of the total magnetic resonance signal due to molecular self-diffusion alone! The SNR was further degraded by 75%, compared to the pure phase encode case, because a large filter width of 5.3 kHz was required. These signal losses are difficult to overcome, and are the two principal reasons why high resolution thin film imaging with conventional frequency encoding is extremely challenging.

STRAFI is a multi echo pure frequency encoding method and therefore provides a ready benchmark for spin echo SPI. High resolution depth profiles [4] of an alkyd coating with cobalt catalyst and solvent have been obtained with a nominal pixel resolution of 6.5 μm in 30 min with STRAFI [4]. The SNR determined from the published figure was not less that 70. The efficiency (Υ) of the measurements can be calculated [18] from the following equation:

$$\Upsilon = \frac{\mathrm{SNR}/\Delta x}{\sqrt{T_\mathrm{T}}}, \tag{12}$$

where Δx is the pixel size and T_T is the total imaging time. The comparison is of necessity rough because of the dissimilar experimental systems. In the case of the polyurethane coating experiment (Fig. 6 and Table 2) the measured efficiency was 2. For the alkyd coating with cobalt catalyst and solvent an efficiency of 2 was calculated from the result of [4]. One should, however, note that the STRAFI SNR is achieved by collecting and averaging a very large number of echoes. Each STRAFI image is therefore implicitly weighted by a variety of relaxation times along with diffusion attenuation. These effects, particularly for inherently multiexponential relation behavior, will be difficult to separate. The spin echo SPI result was derived from images generated from the first echo in the multi echo acquisition. Subsequent echoes may be logically used for relaxation time mapping.

3.7. Relaxation time and diffusion coefficient mapping

Quantitative MRI will usually require spatial resolution of proton density and relaxation times. In Figs. 8 and 9 T_2-weighted depth images are displayed for the polymer latex emulsion and nafion film. Eight echoes were collected for the polymer latex emulsion, since it has a reasonably long T_2 (Table 1). Four echoes were collected for the nafion film. The T_2 curves represented in Figs. 10A and B are spatially resolved exponential

Table 2
Pulse sequence parameters

	Line width (Hz)	FW (Hz)	t_p (ms)	TE (ms)	TR (ms)	FOV (μm)	SNR[a]
Nafion	100	400	6	13.6	500	270	57
Polyurethane coating	100–1000	1200	6	13.6	750	313	49
Polymer latex emulsion	80–200	400	3.5	9.0	1000	640	42
Nafion[b]	100	400	5	11.6	500	330	29
Doped water[c]	100	400	6.3	30	250	298	24

[a] SNR values were calculated only for images derived from the first echo.
[b] Parameters correspond to T_2-weighting measurements of nafion film (Fig. 9).
[c] The doped water sample was used for diffusion mapping measurements.

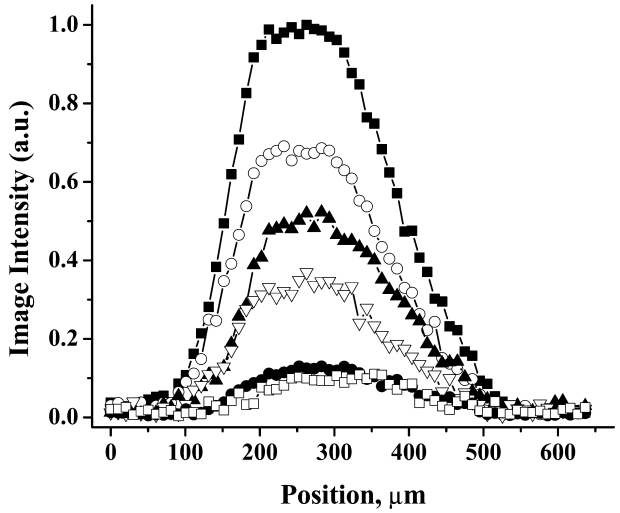

Fig. 8. Relaxation time mapping of polymer latex emulsion polymerization. 1D T_2-weighted depth images obtained for the polymer latex emulsion sample after 30 min of curing. The sample thickness was approximately 250 μm. Images (■, ○, ▲, ▽, ●, and □) were obtained for TE = 9, 18, 27, 36, 45, and 54 ms. The image acquisition time was 4.5 min.

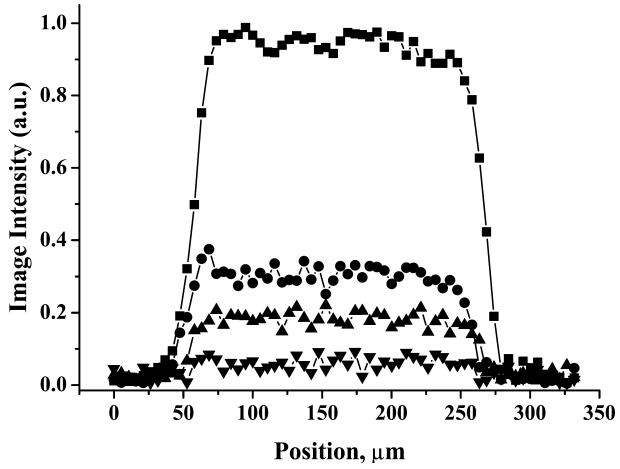

Fig. 9. Relaxation time mapping of a nafion film. 1D T_2 weighted depth images were obtained (■, ●, ▲, and ▼) for TE = 11.6, 23.2, 34.8, and 46.8 ms. As nafion is a static sample, with depth invariant T_2 all depth images have uniform image intensity.

decays for both systems. The polymer latex emulsion relaxation curves are plotted for three different regions (Fig. 8). Analysis of the relaxation curves allows one to extract spatially resolved T_2 values. The polymer latex emulsion T_2 values were 27.5, 24.3, and 19.7 ms for the three different regions. For the nafion film sample, the T_2 relaxation value was spatially uniform at 11.0 ms (Fig. 9).

The large variation of B_1 within the sensitive spot might suggest that even the XY-4 phase cycle may not be able to measure good T_2 decays. Spatially resolved T_2 measurements, for uniform samples, were experimentally confirmed two different ways. There is a good agreement between the values of the spin–spin relaxation time constant obtained from bulk relaxation measurements (Table 1) and the values extracted from analysis of T_2-weighted depth images. The bulk measurements were performed with CPMG and a large volume resonator with uniform B_1.

Additional bulk relaxation time measurements were undertaken with a large, 3 cm × 3 cm, and small, 2 mm diameter nafion sheet centered over the surface coil probe. The XY-4 echo measurement in each case reproduced the volume resonator T_2 measurement of these samples, and the depth resolved measurement. The 2 mm diameter sample experienced minimal B_1 field dispersion and a successful measurement is no surprise. The 3 cm × 3 cm sample, however, experienced a very large dispersion of the B_1 field—it is physically larger than the surface coil probe. In this case the Crawley, Wood, and Henkelman spoiling scheme Fig. 2B is essential even in a bulk measurement.

The T_2 lifetime of the nafion film (Table 1) did not permit more than 4 useable echoes (Fig. 9), to be collected in each imaging echo train. Decreasing the echo time will permit more experimental data points, as will executing the same basic measurement with variable TE. The using of a shorter TE will in any case increase the magnetic resonance signal and thereby decrease the total acquisition time. This is very important, especially in the case of observation of dynamic phenomenon in thin films.

The minimum TE is determined by the maximum value of the magnetic field gradient and the gradient rise time. The sequence used in this work (Fig. 2C) has quite a low gradient duty cycle, less than 10% of the maximum. This will permit us to employ magnetic field gradients which are 100 G/cm with a rise time of approximately 150 μs in future work with the same magnetic field gradient coil. For a nominal resolution of 5 μm, this will permit TE to be reduced by more than a factor of 4.

The spin echo SPI method may be readily adapted for diffusion mapping. For diffusion mapping the pulse sequence of Fig. 2C was modified. The spoil gradients on the x-axis were replaced by bipolar diffusion gradients. A micro capillary containing doped water was used as a model sample. The width of the micro capillary along the x-axis was 0.4 cm (Table 1) and therefore one anticipates that self-diffusion along the x-axis will be unrestricted. Fig. 11 shows diffusion-weighted depth images from the micro capillary. Diffusive decay of the local image intensity is represented in Fig. 11. A plot of the dependence of the image intensity versus G_x^2 is linear on a semi logarithmic scale as expected. The diffusion coefficients may be extracted from the slope of the plot by using Eq. (6). The self-diffusion coefficients for positions 96, 147, and 164 μm of the 1D depth images

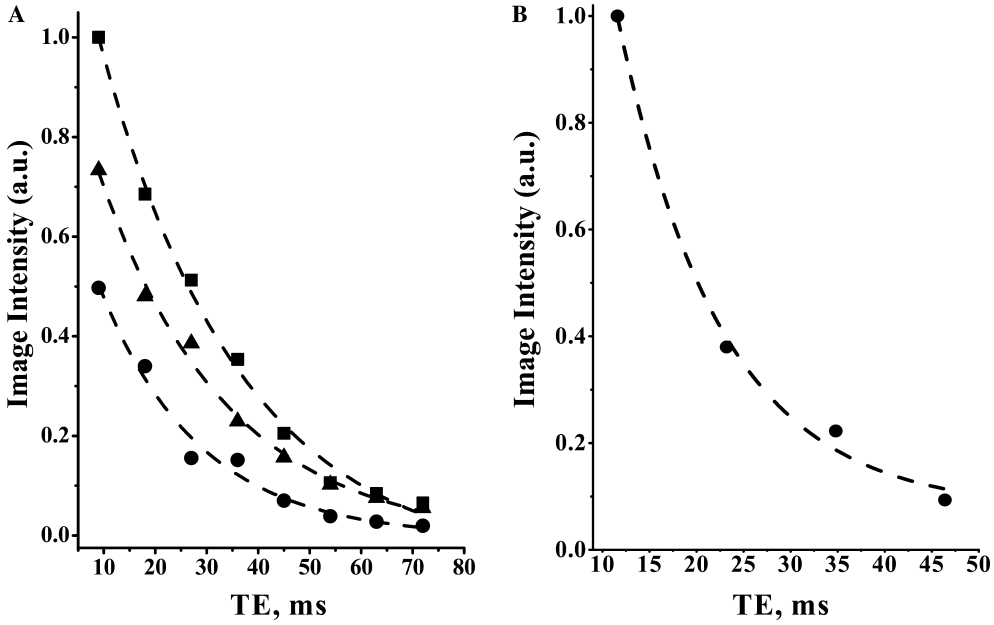

Fig. 10. (A) T_2 decay curves extracted from selected positions in the polymer latex emulsion depth images Fig. 8. Data points (■, ▲, and ●) correspond to positions 150, 260, and 330 μm in Fig. 8. The T_2 values at these positions were 27.5, 24.3, and 19.7 ms, respectively. (B) T_2 decay curve extracted from nafion depth images of Fig. 9. As nafion is a static sample it has a spatially invariant T_2, 11.0 ms.

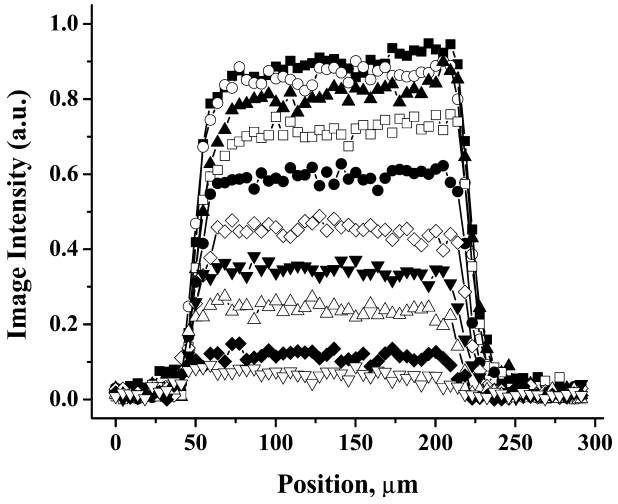

Fig. 11. Depth imaging of the micro capillary sample with diffusion weighting. Sixteen equidistant gradient steps from zero to maximum were employed. The maximum value of the diffusion gradient was 27 G/cm. Depth images corresponding to the first 10 diffusion gradient values are presented. All profiles have a rectangular shape with a uniform signal intensity distribution. The change in image intensity is due to diffusion weighting given by Eq. (4). The sample thickness was approximately 200 μm.

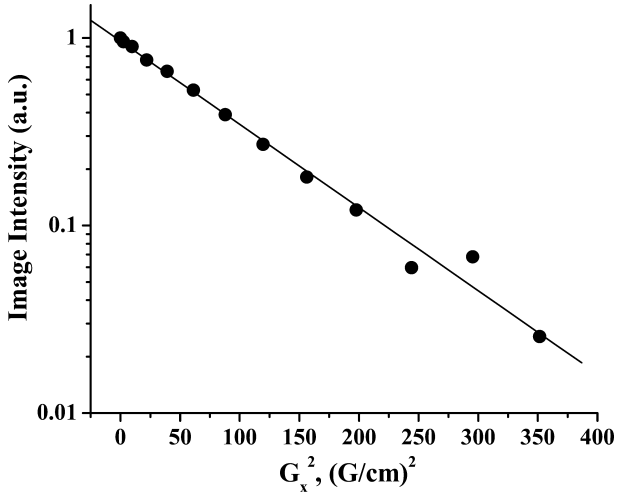

Fig. 12. Local attenuation of image intensity with diffusion weighting for the images of Fig. 11. Gradient G_x was employed as the diffusion gradient. The value of the self-diffusion coefficient, x-direction, was 1.58×10^{-9} m^2/s.

(Fig. 12) were $1.49 \pm 0.04 \times 10^{-9}$, $1.58 \pm 0.05 \times 10^{-9}$, and $1.53 \pm 0.06 \times 10^{-9}$ m^2/s at 10 °C. As expected they are spatially uniform within experimental error. The values are in reasonable agreement with the literature value, $1.67 \pm 0.25 \times 10^{-9}$ m^2/s [25] at similar temperatures. A depth resolved self-diffusion coefficient measurement for the nafion thin film reveals a spatially uniform water self-diffusion coefficient of $1.09 \pm 0.03 \times 10^{-9}$ m^2/s, at 10°C.

4. Conclusion

A new double phase encode multiple spin echo SPI sequence was developed for high resolution 1D depth imaging of thin film liquid-like samples. The method is sufficiently rapid to permit time resolved imaging of

dynamic samples. Resolution loss due to non-orthogonality of the phase encoding gradient and the planar sample may be avoided by using linear combinations of orthogonal phase encode gradients.

The absence of the magnetic field gradient during the signal acquisition ensures minimal diffusion attenuation. Optimal digital filtering, further ensures high SNR. Small modifications to the method permit T_2 and diffusion coefficient mapping.

Future work will explore the absolute resolution limits of the method using linear combination of all three magnetic field gradients in addition to measurements of diffusion and flow in all three gradient dimensions for amenable thin film samples. The use of higher strength magnetic field gradients will permit shorter echo times and consequently better SNR and more accurate T_2 mapping of shorter T_2 samples.

We anticipate that these factors, combined with the relatively short acquisition time of the experiment will ensure the method will be quite general in application and amenable to the study of a wide variety of thin film samples.

5. Experimental

Spin echo SPI experiments were carried out on a Nalorac (Martinez, CA) horizontal bore superconducting magnet at 100 MHz. All imaging measurements employed a Nalorac micro gradient set with maximum gradient values of 27.5 G/cm. Gradient G_y was chosen to be the principal phase encoding gradient. Gradient G_z was used as the second phase encoding gradient and G_x was applied as a spoil gradient. The gradient set was water cooled and driven by Techron 8710 gradient amplifiers. All images were obtained on an Apollo (Tecmag, Houston, TX) console. All measurements were performed at ambient temperature and humidity.

Bulk relaxation time measurements employed a commercial quadrature birdcage probe (Morris Instruments, Ottawa, ON). All imaging measurements utilized a single channel home built surface coil probe. The solenoid-like surface coil was constructed on a 1 cm diameter teflon form. Three turns of Gauge 25 wire with teflon tubing as a dielectric was wound on the form and tuned to 100 MHz with two capacitors in a standard series-parallel tank circuit. The form was then mounted on a 1.27 cm thick teflon sheet and placed in a shielded plexiglass tube. Three adjustment screws were provided to level the surface coil. The surface coil probe was excited with a 2 kW AMT (Brea, CA) 3445 RF amplifier. True 90° pulse lengths, typically 13 μs, were determined for small nafion samples centered on the surface coil probe. All pulse widths were stable and reproducible.

The nafion film [26] (Sigma–Aldrich Canada, Oakville, Ontario, Canada), polyurethane coating (Flecto Coatings, Richmond, BC, Canada), and polymer latex emulsion (Lepage's, Brampton, Ontario, Canada) were chosen as representative planar samples with different chemical and MR properties. The relaxation time parameters, and the physical sizes of the investigated thin films are reported in Table 1.

The choice of experimental parameters for spin echo SPI measurements was based on the values of the relaxation times of the samples. Experimental timing parameters are reported in Table 2. The optimal filter width for this technique is equal to the sample line width. The values of TE were chosen based on the required image resolution and T_2 value. The repetition time (TR) was maintained at $5T_1$ in all measurements. The field-of-view was chosen based on the film thicknesses with typical values of 290–600 μm (Table 2). Quadrature phase cycling was employed in all 1D and 2D spin echo SPI measurements. The gradient duty cycle for all measurements was less than 3%.

Pseudo-FID measurements employed a saturated nafion sheet. The 80 FIDs were obtained for 80 different (from 1 to 80 μs) pulse widths. Each FID has 1024 points. The TR was 1 s and the filter width 400 Hz. The final pseudo-FID curve was obtained through Fourier transformation (FFT) of each FID with the absolute value of the peak maximum plotted the versus the pulse width.

Sixty-four k-space data points were collected for 1D imaging measurements and 64 by 64 matrix points were collected for 2D imaging measurements. Images were obtained through FFT of the k-space data. No zero filling or line broadening filtering was employed in the image reconstruction.

MatLab 6.5 (The MathWorks, Natick, MA, US) and IDL 5.6 (Research System, Boulder, CO, US) were used for magnetic field and magnetic resonance signal calculation. Calculations were executed on an Intel Pentium III, 800 MHz computer (Dell Canada).

The nafion film was used as a 2D phantom to examine the sensitive spot. The nafion film was kept in distilled water for 10 days prior to measurements. During the experiment, nafion was sandwiched between two microscope slides to ensure constant water content. The FOV was 2×2 cm, 64×64 pixels with a t_p of 0.5 ms and TE of 2 ms. The TR was 300 ms and the total acquisition time 6 h with 16 signal averages (Fig. 4C) and 12 h with 32 signal averages (Fig. 4D). The gradients G_x and G_z, 5 G/cm maximum each, were used for lateral 2D spin echo SPI imaging. The nominal pixel resolution was 0.31 mm, with a single echo collected. The filter width was 400 Hz (Table 2).

The image acquisition time, 16 averages, was 8 min for 1D depth images of the nafion film. The nominal pixel resolution was 4.2 μm with 8 echoes collected. Only the first four echoes were used for image reconstruction. The angle α was set at 0.35°.

The polyurethane coating was applied on a glass substrate immediately prior to measurement. Depth images of the polyurethane coating were acquired over a period of 20 h. The acquisition time for a single profile 64 points, 16 averages, was 16 min, 8 echoes were collected. Only the first four echoes were used for image reconstruction. The nominal pixel resolution was 4.9 μm, with angle α set at 0.125°.

The polymer latex emulsion was applied to the interfacial surfaces of two pieces of balsa wood prior to experimentation. Depth images, 4 averages, were acquired over 12 h. The acquisition time for a single profile was 4.5 min. The nominal pixel resolution was 10 μm, with 8 echoes collected. The secondary phase encode gradient was not used.

The optimal filter width for the nafion and polymer latex emulsion samples was too small for the Apollo digital filter, consequently a larger value was employed. For the polyurethane coating the maximal line width was used as the filter width because T_2^* was decreasing (Table 1) during investigation of this sample.

Doped water (10 mM $CuSO_4$) in a micro capillary (Friedrich and Dimmock, Millville, NJ) was used for diffusion mapping. Sixteen equidistant steps in diffusion gradient (G_x) from zero to 27.5 G/cm were employed. The diffusion-weighted depth images had a nominal pixel resolution of 4.5 μm, with an angle α of 0.35°. Four signal averages were collected for a total experimental time of 24 min. The images were derived from the first echo.

Acknowledgments

B.J. Balcom thanks NSERC of Canada for equipment and operating grants in addition to a Steacie fellowship (2000–2002). B.J. Balcom also thanks the Canada Chairs program for a Canada Research Chair in MRI of Materials. We thank Dr. Elizabeth McCord of DuPont CRDS for suggesting the original thin film problem. We thank Andrew Marble for assistance with the MatLab simulations'.

References

[1] H. Bubert, H. Jenett, Surface and Thin Film Analysis: A Compendium of Principles, Instrumentation, and Applications, Wiley-VCH Verlag, 2002.
[2] P.J. McDonald, Stray field magnetic resonance imaging, Prog. Nucl. Magn. Reson. Spectrosc. 30 (1997) 69–99.
[3] P.M. Glover, P.J. McDonald, B. Newling, Stray-Field imaging of planar films using a novel surface coil, J. Magn. Reson. 126 (1997) 207–212.
[4] P.M. Glover, P.S. Aptaker, J.R. Bowler, E. Ciampi, P.J. McDonald, A novel high gradient permanent magnet for profiling of planar films and coatings, J. Magn. Reson. 139 (1999) 90–97.
[5] J. Godward, E. Ciampi, M. Cifelli, P.J. McDonald, Multidimensional imaging using Stray-Field and pulsed gradients, J. Magn. Reson. 155 (2002) 92–99.
[6] P.T. Callaghan, L.C. Forde, C.J. Rofe, Correlated susceptibility and diffusion effects in NMR microscopy using both phase-frequency encoding and phase–phase encoding, J. Magn. Reson. 104 (1994) 34–52.
[7] D.I. Hoult, Rotating frame zeugmatography, J. Magn. Reson. 33 (1979) 183–197.
[8] S. Choi, X.-W. Tang, D.G. Cory, Constant time imaging approaches to NMR microscopy, Int. J. Imag. Syst. Tech. 8 (1997) 263–276.
[9] M.T. Vlaardingerbroek, J.A. der Boer, Magnetic Resonance Imaging: Theory and Practice, Springer-Verlag, Berlin, 1996.
[10] C.S. Boschk, J.J.H. Ackerman, In-Vivo Magnetic Resonance Spectroscopy II: Localization and Spectral Editing, NMR 27, Springer-Verlag, Berlin, 1992, pp. 4–23.
[11] D.K. Chen, Field and Wave Electromagnetics, Addison-Wesley Publishing Company, Inc, Reading, MA, 1990.
[12] B.J. Balcom, SPRITE imaging of short relaxation time nuclei, in: B. Blumich, W. Kuhn (Eds.), Spatially Resolved Magnetic Resonance: Methods. Materials, Medicine, Biology, Rheology, Geology, Ecology, Hardware, Wiley-VCH, Weinheim, 1998, pp. 75–86.
[13] P.J. Prado, B. Blumich, U. Schmitz, One-dimensional imaging with a palm-size probe, J. Magn. Reson. 144 (2000) 200–206.
[14] M.S. Conradi, High-resolution imaging of a ceramic, J. Magn. Reson. 93 (1991) 419–422.
[15] A.A. Maudsley, Modified Carr–Purcell–Meiboom–Gill sequence for NMR Fourier imaging applications, J. Magn. Reson. 69 (1986) 488–491.
[16] T. Gullion, The effect of amplitude imbalance on compensated Carr–Purcell sequence, J. Magn. Reson. 101 (1993) 320–323.
[17] A.P. Crawley, M.L. Wood, R.M. Henkelman, Elimination of transverse coherences in FLASH MRI, Magn. Reson. Med. 8 (1988) 248–260.
[18] E.M. Haacke, R.W. Brown, M.R. Thompson, R. Venkatesan, Magnetic Resonance Imaging: Physical Principles and Sequence Design, Wiley, New York, 1999.
[19] B. MacMillan, A.R. Sharp, R.L. Armstrong, NMR relaxation in nafion—the low temperature regime, Polymer 40 (1999) 2481–2484.
[20] B. MacMillan, A.R. Sharp, R.L. Armstrong, An NMR investigation of the dynamical characteristics of water absorbed in nafion, Polymer 40 (1999) 2471–2480.
[21] D.A. Seeber, J.H. Hoftiezer, W.B. Daniel, M.A. Rutgers, C.H. Pennington, Triaxial magnetic field gradient system for microcoil magnetic resonance imaging, Rev. Sci. Inst. 11 (2000) 4263–4272.
[22] D.A. Seeber, R.L. Cooper, L. Ciobanu, C.H. Pennington, Design and testing of high sensitivity microreceiver coil apparatus for nuclear magnetic resonance and imaging, Rev. Sci. Inst. 4 (2001) 2171–2179.
[23] A. Ouriadov, B. MacMillan, Y. Cheng, B.J. Balcom, Magnetic resonance imaging of layered materials using spin echo SPI, in: 6th International Conference on Magnetic Resonance Microscopy, 2001, p. 35.
[24] P. Bernada, S. Stenstrom, S. Mansson, Experimental study of the moisture distribution inside a pulp sheet using MRI. Part II: drying experiments, J. Pulp Paper Sci. 12 (1998) 380–388.
[25] D. Eisenberg, W. Kauzman, The Structure and Properties of Water, Oxford University Press, Oxford, 1969.
[26] A.J. Hopfinger, K.A. Mauritz, Theory of the structure of ionomeric membranes, Compr. Treatise Electrochem. (1981) 512–535.